Mineral Processing and Extractive Metallurgy Review
An International Journal

ISSN: (Print) (Online) Journal homepage: https://www.tandfonline.com/loi/gmpr20

Conceptual Process Development for the Separation of Thorium, Uranium, and Rare Earths from Coarse Coal Refuse

Deniz Talan, Qingqing Huang, Liang Liang & Xueyan Song

To cite this article: Deniz Talan, Qingqing Huang, Liang Liang & Xueyan Song (2022): Conceptual Process Development for the Separation of Thorium, Uranium, and Rare Earths from Coarse Coal Refuse, Mineral Processing and Extractive Metallurgy Review, DOI: 10.1080/08827508.2022.2064855

To link to this article: https://doi.org/10.1080/08827508.2022.2064855

Published online: 17 Apr 2022.

MINERAL PROCESSING AND EXTRACTIVE METALLURGY REVIEW
https://doi.org/10.1080/08827508.2022.2064855

Taylor & Francis
Taylor & Francis Group

Conceptual Process Development for the Separation of Thorium, Uranium, and Rare Earths from Coarse Coal Refuse

Deniz Talan [a], Qingqing Huang[a], Liang Liang[b], and Xueyan Song[b]

[a]Department of Mining Engineering, West Virginia University, Morgantown, West Virginia, US; [b]Department of Mechanical and Aerospace Engineering, West Virginia University, Morgantown, West Virginia, US

ABSTRACT

Increasing disruption in the rare earth supply chain creates an urgency to develop alternative resources, in which utilization of coal-based materials presents great potential. Nevertheless, environmental control is a significant challenge in rare earth extraction processes. This study was conducted to contribute to the limited information on removing thorium and uranium from rare earths while coal-based products are used as feedstock. The laboratory studies suggested that the selective precipitation and solvent extraction approach yields the most favorable separation performance. Complete thorium precipitation was achieved around a pH value of 4.8. Due to the close precipitation pH ranges of uranium and rare earths, further separation by solvent extraction was applied to achieve an enhanced separation. Based on a Box-Behnken experimental design, the effect of extractant concentration, pH, strippant concentration, and O/A ratio was investigated. Best separation performance was achieved using 50 v% TBP at a pH of 3.5 with an O/A ratio of 3 and 1 mol/L H_2SO_4, which resulted in 1.8% uranium and 73.4% rare earth extraction. The extraction and precipitation behavior of the elements were further assessed with the distribution ratio, separation factor, thermodynamic parameters, and species distribution diagrams to provide a thorough understanding of the separation mechanisms. The results were statistically analyzed, and a model was developed to predict uranium recovery. The developed experimental protocol was validated using a rare earth oxalate sample produced at the pilot-scale processing facility. Finally, a conceptual process flow-sheet was developed to effectively separate radionuclides while producing rare earth oxide products.

KEYWORDS

Rare earth elements; thorium and uranium separation; coal; fundamental studies; process development

1. Introduction

Rare earth elements display unique physical and chemical properties, making them vital for numerous industries. They are heavily used to manufacture various electronics, batteries, magnets, military and defense systems and equipment, medical treatment drugs, etc. (Akcil et al. 2018; Baek et al. 2016; Binnemans et al. 2013; Ismail et al. 2019). Although they have a high abundance in the Earth's crust, rare earth element extraction has always been a challenge due to limited economically feasible deposits. Nowadays, rare earth-dependent product consumption has increased significantly due to technological advancements. As global rare earth consumption increases, the search for alternative sources to confront rare earth elements' supply and demand balance has gained extreme significance. Within this context, new deposits have been found in Canada, the United Kingdom, Estonia, and Greenland (Suli et al., 2017), and new operations have been started in India, Brazil, Vietnam, Russia, and Malaysia to produce rare earths as a by-product of rutile, zircon, magnesia, and cassiterite plants (Paulick and Machacek 2017; Van Gosen et al. 2017). Rare earth extraction from electronic waste has made the utilization of millions of tons of electrical and electronic waste generated each year feasible (Erust et al. 2021; Ferron and Henry 2015). Alternatively, bauxite residue (red mud) has a considerable rare earth concentration, particularly high in scandium (Akcil et al. 2018). Other secondary sources, apatite, cheralite, eudialyte, and loparite are especially rich in gadolinium, terbium, dysprosium, holmium, erbium, thulium, ytterbium, lutetium, and yttrium (Dutta et al. 2016; Schreiber et al. 2016). Moreover, phosphate rock and its by-products (i.e. phosphogypsum, phosphoric acid, phosphoric acid sludge) are reported to have a rare earth concentration varying from 100 to 1000 ppm (Al-Thyabat and Zhang 2015; Eskanlou and Huang 2021). Abaka-Wood and his coworkers (2021) recently performed comprehensive research on the characterization of rare earth elements from bornite and chalcopyrite tailings, which showed that rare earths are generally locked within the particles and tend to associate with bastnaesite/stetindite-silicate or monazite/stetindite-silicate minerals.

In addition to these promising feedstocks, coal and coal-based materials (e.g. fly ash, bottom ash, acid mine drainage, and its treatment products, and coal refuse) have also demonstrated their potential via laboratory and pilot-scale applications and investigations (; Honaker et al. 2016; Hower et al. 2016; Huang et al. 2018, 2019; McLellan et al. 2014; Zhang and Honaker 2018). The average rare earth element content in coal has been estimated as 69 ppm on a whole mass basis based on studies conducted in different geological locations (Eskanazy 1987; Hu et al. 2006; Huang et al. 2019; Karayigit et al. 2000; Ketris and Yudovich 2009; Wagner and Matiane 2018). On the

CONTACT Qingqing Huang qingqing.huang@mail.wvu.edu Department of Mining Engineering, West Virginia University, 365 Mineral Resources Building, Evansdale Drive, Morgantown 1374, West Virginia, US

other hand, given them being mostly nonvolatile, rare earth enrichment is reported to be higher in coal ash samples (i.e. fly ash and bottom ash) as well as coal refuse samples, with a content of 445 ppm and up to 500 ppm, respectively (Kawatra 2020; Pan et al. 2019; Yang et al. 2020). The occurrence of rare earth elements in coal and its by-products have been investigated. The studies conducted by Honaker and his coworkers (2016, 2014) indicated that the rare earth element distribution in coal is associated with the incombustible material and seen in the form of monazite, xenotime, and bastnaesite, with the particle size range varying between 1–10 μm or even smaller. The study conducted by Pan et al. (2019) reported similar results and stated that rare earths enrichment increases as the particle size decreases. Considering the increase in the world's energy need due to continued population and industrialization, the use of coal, and consequently, the production of coal by-products will continue proportionately. Therefore, the proper utilization of coal and coal by-products provides an excellent opportunity to supply rare earth elements and facilitate a circular economy.

However, rare earth extraction processes cause significant environmental issues by producing radioactive streams due to the association of naturally occurring radioactive materials, such as thorium and uranium. Both conventional and unconventional rare earth sources contain a detectable amount of radioactive matter (Pillai 2007). While traditional rare earth minerals (e.g. monazite, bastnasite, xenotime) can contain thorium and uranium dioxides with concentrations as high as 20 and 16 wt%, separately (Van Gosen et al. 2017), the average thorium and uranium contents in coal are approximated as 3.2 and 2.1 ppm (Finkelman 1999), which is either associated with elements in the coal itself or within the minerals that are part of coal formation (Cooper 2005; Dai and Finkelman 2018; Lange et al. 2017; Papastefanou 2007). In addition to thorium and uranium, their decay products such as radium and radon and some condensed elements with high volatility (i.e. As, Cd, Cu, Pb, etc.) may present in coal-related materials as well (Parzentny and Rog 2019; USGS, 1997). Although the concentrations of thorium and uranium in coal and coal by-products are considerably lower than the primary sources of rare earths, the radioactive elements can be substantially enriched along with the processing stages, which may accumulate on the soil or transfer into water streams, thus creating concerns for living organisms and the ecosystem (Abdel-Sabour 2014). Therefore, it is crucial to ensure that the extraction processes are environmentally benign due to the nature of the occurrence of rare earths (Al-Areqi, Majid and Sarmani 2014; Ault, Krahn and Croff 2015; Haque et al. 2014; Valkov et al. 2014; Wang et al. 2017; Zhang, Zhao and Schreiner 2016).

Precipitation and solvent extraction are two of the most widely used separation methods for extracting rare earths. These two techniques have also been proven to efficiently remove thorium and uranium under controlled operating conditions. During precipitation, radionuclides are removed from the solution by forming less soluble compounds with a chemical reagent, and the mechanism takes advantage of the differing precipitation pH ranges of the elements. It was stated in Kim and Ossae's (2012) study that dissolved species of thorium, uranium, and rare earth metals in acidic solutions may be separated by pH adjustment. As indicated in Zhu and his coworkers' study (2015), in chloride media, thorium's precipitation happens first at a pH range between 2.5–5.5. Following thorium, uranium precipitation occurs at approximately 5.5–7; later, the precipitation of rare earths is seen between pH 6.8–8 (Langmuir 1978; Zhu, Pranolo and Cheng 2015). However, changes in the precipitation pH ranges are expected depending on the solution medium, elemental concentration, ionic species, and the concentration of the precipitation chemicals used. For example, in sulfate media, the precipitation of thorium, uranium, and rare earths is seen at lower pH values, and in nitric acid media, the opposite phenomenon, an increased precipitation pH range, is observed (Garcia et al. 2020; Zhu, Pranolo and Cheng 2015).

Although precipitation is known to be effective, simple, and less costly, due to the complex nature of rare earth-bearing minerals, additional techniques are often needed to achieve improved separation performance. Solvent extraction has been the most extensively used method for purification due to its ability to handle large volumes of aqueous solutions (Hidayah and Abidin 2017). It has also been an effective technique to remove hazardous matters from rare earth elements (Brown and Sherrington 1979). The solvent extraction mechanism is based on transferring ions from an aqueous phase to an organic phase, which is then stripped with acids or DI water to recover ions back into the aqueous phase (Braatz, Antonio and Nilsson 2017; Peramaki 2012). One of the crucial parameters in the solvent extraction process is the type and concentration of the organic extractants since the efficiency of the process heavily depends on the extractant's ability to transfer metal ions between two immiscible phases (Hidayah and Abidin 2017; Zhou et al. 2018). Organic phosphorus acid, carboxylic acid, amine types extractants, and sulfoxide are some of the commercially used extractant types which have been proved to be effective for the separation of radioactive elements while present with rare earths (Belova et al. 2015; Giri and Nath 2016; Gupta, Malik and Deep 2002; Kuang et al. 2017; Palmieri, 2011; Zhu, Pranolo and Cheng 2015).

Amaral and Morais (2010) studied the synergetic effect of primary and tertiary amine (Primene JM-T and Alamine 336) extractants to remove thorium and uranium from sulfuric leach liquor generated from a monazite sample. In another study, Hughes and Singh (1980) used a secondary amine (Adogen 283) to remove thorium from monazite, and both studies achieved >99% extraction recoveries which showed the effective application of amine type extractants. Gupta, Malik and Deep (2002) investigated thorium and uranium separation from rare earths using Cyanex 923. Likewise, Nasab, Sam and Milani (2011) studied thorium removal using Cyanex 272 and Cyanex 302. Both studies achieved satisfactory extraction performance; however, the industrial application of the Cyanex series has not been found since Cyanex extractants require high acidity, making the process infeasible from an economic standpoint. Widely-known conventional extractants, such as diethylhexyl phosphoric acid (D2EHPA) and tributyl phosphate (TBP), are also indicated as effective extractants for thorium and uranium separation. Extraction reactions of thorium and uranium when an organophosphorus extractant is

used are given in reactions 1 and 2. However, the use of TBP is restricted to the extraction from nitrate and chloride media (Gupta, Malik and Deep 2002).

$$UO_2^{2+} + 2NO_3^- + 2X \rightarrow UO_2(NO_3)_2.2X \quad (1)$$

$$Th^{4+} + 4NO_3^- + 3X \rightarrow Th(NO_3)_4.3X \quad (2)$$

Despite provided effectiveness of solvent extraction for thorium and uranium removal, most of these extractants are also effective for extracting rare earths (Agarwal, Safarzade and Galvin 2018; Zhu, Pranolo and Cheng 2015). Therefore, it is essential to develop a unique experimental scheme for the desired selectivity and separation efficiency tailored to the system. For example, the application of acidic organophosphorus extractant, D2EHPA, to extract rare earth elements has been widely studied, and the extraction mechanism follows the reaction given below (Reddy, Prasada Rao and Damodaran 1995). However, it was observed that with an increase in the solution acidity and the rare earth chloride concentration, in addition to the typical extraction mechanism, extraction of rare earth chlorocomplexes may appear (reaction 4).

$$M^{3+} + 3(HX)_2 \rightarrow M(HX_2)_3 + 3H^+ \quad (3)$$

$$M^{3+} + 3Cl^- + \frac{3}{S}(HX)_s \rightarrow MCl_3.3HX \quad (4)$$

where $(HX)_2$ and M^{3+} refer to D2EHPA and rare earth ions, separately. S refers to the mean degree of D2EHPA polymerization, which lies between 2 and 3. Typically, the extraction of rare earths with D2EHPA in a chloride medium increases with an increase in their atomic number, and it was reported that the application of D2EHPA in chloride media is more desirable for rare earth production (Reddy, Prasada Rao and Damodaran 1995). For that reason, the use of D2EHPA in this study was eliminated.

To date, the environmental prospect of rare earth mining caused by the occurrence of radionuclides has not been thoroughly explored. Most of the investigations conducted in this regard considered the conventional sources of rare earths. The studies on the separation of these hazardous elements and rare earths from newly identified sources are noticeably limited. Since coal and its by-products are identified as potential sources for rare earth elements, understanding their environmental aspect and developing an environmentally sound process has utmost importance, considering the possible implementation of such an approach to a commercialized operation. Thus, this study was performed to examine the separation performance of thorium, uranium, and rare earths from a coarse coal refuse sample via selective precipitation and solvent extraction. Besides experimental testing, the precipitation and extraction behaviors of the elements were examined thoroughly with respect to the equilibrium and thermodynamic studies. The separation performance was also studied by various operating parameters, namely, feed solution pH, extractant concentration, organic to aqueous (O/A) ratio, and stripping agent concentration. The statistical analysis was performed based on the test findings to investigate the impact of each operating parameter, and an in-depth discussion was provided regarding the interacting effect of each operating parameter. In the end, a conceptual process flowsheet was designed consisting of five unit operations, and its technical feasibility was validated with a rare earth oxalate sample produced at a pilot-scale rare earth production plant.

2. Experimental

2.1. Sample and materials

The laboratory studies were performed with a synthetic solution following the elemental composition of a strip solution originating from a pilot-scale rare earth processing plant operating in Eastern Kentucky. The original strip solution was produced from coarse coal refuse, which was subjected to hydrochloric acid (HCl) leaching, solvent extraction using di-(2-Ethylhexyl) phosphoric acid (DEHPA), and striping with 6 mol/L HCl. The synthetic solution was decided to be used due to the shortage in the original strip solution. The total rare earth element concentration of the solution was 37.04 mg/L, which primarily consisted of cerium (14.47 mg/L), neodymium (9.03 mg/L), yttrium (3.09 mg/L), samarium (2.67 mg/L), and gadolinium (2.01 mg/L). The rest of the rare earth elements had concentrations changing between 0.01 to 1.91 mg/L. To prepare the strip solution containing 37.04 mg/L of total rare earths, 0.50 mg/L of thorium, and 0.86 mg/L of uranium, standard inductively coupled plasma (ICP) solutions with a content of 1000 ppm were purchased from Ricca Chemical and used. On the other hand, total major metal concentrations of 73.72 mg/L were achieved using high-grade (>99%) metal chloride salts purchased from Alfa Aesar. The majority of the metal impurities attributed to calcium (55.20 mg/L) and iron (12.85 mg/L) followed by magnesium (2.86 mg/L), aluminum (1.99 mg/L), and potassium (0.82 mg/L). Sodium hydroxide (NaOH) with analar grade was purchased from Merck and used to adjust the solution pH throughout the study. Tributyl phosphate (TBP) diluted in kerosene was applied as the extractant due to its high chemical resistance, physical properties, and extensive use in thorium and uranium extraction (Giri and Nath 2016; Habashi 1997; Zhang, Zhao and Schreiner 2016). Chemical grade TBP and kerosene were purchased from Sigma Aldrich, while sulfuric acid (H_2SO_4) was purchased from Fisher Scientific and used as the stripping agent. All the tests were conducted at room temperature (25°C) using DI water unless otherwise stated. During each test, representative samples taken from the aqueous and solid samples were subjected to rare earth elements and major metal analyses using Spectro Arcos 2 Inductively Coupled Plasma-Optical Emission Spectroscopy (ICP-OES). In addition, thorium and uranium analyses were performed using Perkin Elmer Nexion 2000 Inductively Coupled Plasma-Mass Spectroscopy (ICP-MS).

2.2. Method

2.2.1. Selective precipitation

Based on the exploratory tests conducted earlier (Talan and Huang 2020), solution pH was adjusted to approximately a value of 4.8 to selectively remove thorium using a 2 mol/L

NaOH solution. A sufficient amount of time was given for a complete settling and precipitation when the solid formation was observed. Later, the solution was filtered using filter paper with a pore size of 0.45 µm and precipitated solids were dried in the oven and weighed. Representative samples were taken from the filtrate and solids and subjected to thorium, uranium, rare earth elements, and major metal analyses using ICP-OES and ICP-MS.

Solution chemistry was further studied to investigate the precipitation mechanism of various elements. Species distribution diagrams of selected rare earths (i.e. cerium, neodymium, gadolinium, lanthanum, yttrium), thorium, uranium, iron, and aluminum were constructed using the data generated from OLI Studio software and MINTEQ Version 3.1. The reactions occurring and their respective solubility constants at 25°C are given in Table 1. The ionic strength (I) of the system, indicating the concentration of ions in the solution, was 0.09 following reaction 5. Precipitation mechanisms of the elements were also investigated by saturation index (SI), which shows whether species will stay dissolved or precipitate (reaction 6). Additionally, thermodynamic parameters, including the Gibbs free energy (ΔG, kJ/mol), enthalpy (ΔH, kJ/mol), and entropy (ΔS, J.mol^{-1}.K^{-1}) values, were calculated following the test conditions. While the value of ΔG suggests whether the reaction is spontaneous or not, ΔH indicates if the precipitation reaction is endothermic or exothermic and is directly correlated with ΔG^0, as shown in reaction 7 (Preira et al. 2019).

$$I = \frac{1}{2}\sum_{i=1}^{n} c_i z_i^2 \tag{5}$$

where c_i is the ion concentration (mol/L) and z_i is the ion charges. ½ is included in the equation since both anions and cations are considered.

$$Saturation Index(SI) = \log IAP - logK \tag{6}$$

where IAP is the ion activity product of the species and K is the solubility constant given in Table 1.

$$\Delta G^0 = \Delta H^0 - T\Delta S^0 \tag{7}$$

where T refers to the temperature (K).

2.2.2. Solvent extraction

Following selective precipitation, the filtrate loaded with uranium and rare earths was used as the feedstock for subsequent solvent extraction tests. Two-stage solvent extraction was performed using TBP dispersed in kerosene and H_2SO_4 as the extractant and strippant, respectively. Organic and aqueous phases were mixed for 20 mins that were later separated using a separation funnel. As described previously, representative aqueous samples were taken from each step and analyzed using both ICP-MS and ICP-OES for elemental compositions. The elemental concentration of the organic phase was determined via the mass difference between the feed and raffinate phases.

During solvent extraction, the effect of four influential parameters, namely, extractant concentration (30, 40, 50 v% TBP), feed solution pH (2.5, 3.5, 4.5), strippant (H_2SO_4) concentration (0.5, 1, 2 mol/L) and O/A ratio (1:1, 2:1, 3:1), on the separation performance of uranium from rare earths was investigated. These parameters were determined based on a thorough literature review (Biswas et al. 2013; Jha et al. 2016; Menzies and Rigby 1961; Nasab, Sam and Milani 2011; Xie et al. 2014). In total, 27 tests were performed following a Box-Behnken experimental design to ensure that the number of tests was sufficient to evaluate the significance of each operating parameter (Figure 1). At the end of solvent extraction, the rare earth-containing product stream, organic phase, and uranium-containing streams were generated.

Table 1. Solubility constants of the major reactions occurring within the solution system.

Chemical Reactions	Solubility Constant (log K)
$Th^{4+} + OH^- = Th(OH)^{3+}$	−2.5
$Th^{4+} + 2OH^- = Th(OH)_2^{2+}$	−6.2
$Th^{4+} + 3OH^- = Th(OH)_3^{+}$	−11
$Th^{4+} + 4OH^- = Th(OH)_4$	−17.4
$Th^{4+} + 4OH^- = ThO_2 + 2H_2O$	1.77
$Th^{4+} + Cl^- = ThCl^{3+}$	1.7
$(UO_2)^{2+} + OH^- = (UO_2OH)^{+}$	−5.25
$2(UO_2)^{2+} + 2OH^- = (UO_2)_2(OH)_2^{2+}$	−5.62
$(UO_2)^{2+} + 2OH^- = UO_2(OH)_{2(aq)}$	−12.15
$(UO_2)^{2+} + 2OH^- = UO_2(OH)_2$	5.62
$(UO_2)^{2+} + 2Cl^- = UO_2Cl_2$	−1.1
$(UO_2)^{2+} + Cl^- = UO_2Cl^{+}$	0.17
$Ce^{3+} + OH^- = Ce(OH)^{2+}$	−8.34
$Ce^{3+} + 3OH^- = Ce(OH)_{3(aq)}$	16.00
$Ce^{3+} + 3OH^- = Ce(OH)_3$	19.89
$Ce^{3+} + Cl^- = CeCl^{2+}$	0.57
$Gd^{3+} + OH^- = Gd(OH)^{2+}$	−7.83
$Gd^{3+} + 3OH^- = Gd(OH)_{3(aq)}$	16.00
$Gd^{3+} + 3OH^- = Gd(OH)_3$	15.09
$Gd^{3+} + Cl^- = GdCl^{2+}$	0.30
$La^{3+} + OH^- = La(OH)^{2+}$	−8.81
$La^{3+} + 3OH^- = La(OH)_{3(aq)}$	16.00
$La^{3+} + 3OH^- = La(OH)_3$	20.29
$La^{3+} + Cl^- = LaCl^{2+}$	0.53
$Nd^{3+} + OH^- = Nd(OH)^{2+}$	−8.18
$2Nd^{3+} + 4OH^- = Nd_2(OH)_4^{2+}$	−13.89
$Nd^{3+} + 4OH^- = Nd(OH)_4^{-}$	−37.39
$Nd^{3+} + 3OH^- = Nd(OH)_{3(aq)}$	16.00
$Nd^{3+} + 3OH^- = Nd(OH)_3$	18.09
$Y^{3+} + OH^- = Y(OH)^{2+}$	−7.8
$2Y^{3+} + 2OH^- = Y_2(OH)_2^{4+}$	−14.19
$Y^{3+} + 3OH^- = Y(OH)_{3(aq)}$	16.00
$Y^{3+} + 3OH^- = Y(OH)_3$	17.49
$Y^{3+} + Cl^- = YCl^{2+}$	0.58
$Al^{3+} + OH^- = Al(OH)^{2+}$	−4.99
$Al^{3+} + 2OH^- = Al(OH)_2^{+}$	−10.29
$Al^{3+} + 4OH^- = Al(OH)_4^{-}$	−23.00
$2Al^{3+} + 2OH^- = Al_2(OH)_2^{4+}$	−7.69
$3Al^{3+} + 4OH^- = Al_3(OH)_4^{5+}$	−13.88
$Al^{3+} + 3OH^- = Al(OH)_{3(aq)}$	−16.69
$Al^{3+} + 3OH^- = Al(OH)_3$	7.74
$Al^{3+} + Cl^- = AlCl^{2+}$	−0.39
$Fe^{3+} + OH^- = Fe(OH)^{2+}$	−2.02
$Fe^{3+} + 2OH^- = Fe(OH)_2^{+}$	−5.75
$Fe^{3+} + 4OH^- = Fe(OH)_4^{-}$	−22.7
$2Fe^{3+} + 2OH^- = Fe_2(OH)_2^{4+}$	−2.84
$3Fe^{3+} + 4OH^- = Fe_3(OH)_4^{5+}$	−6.29
$2Fe^{3+} + 3H_2O - 6H^+ = Fe_2O_3$	−1.42
$Fe^{3+} + 3OH^- = Fe(OH)_3$	+38.55
$Fe^{3+} + Cl^- = FeCl^{2+}$	1.48

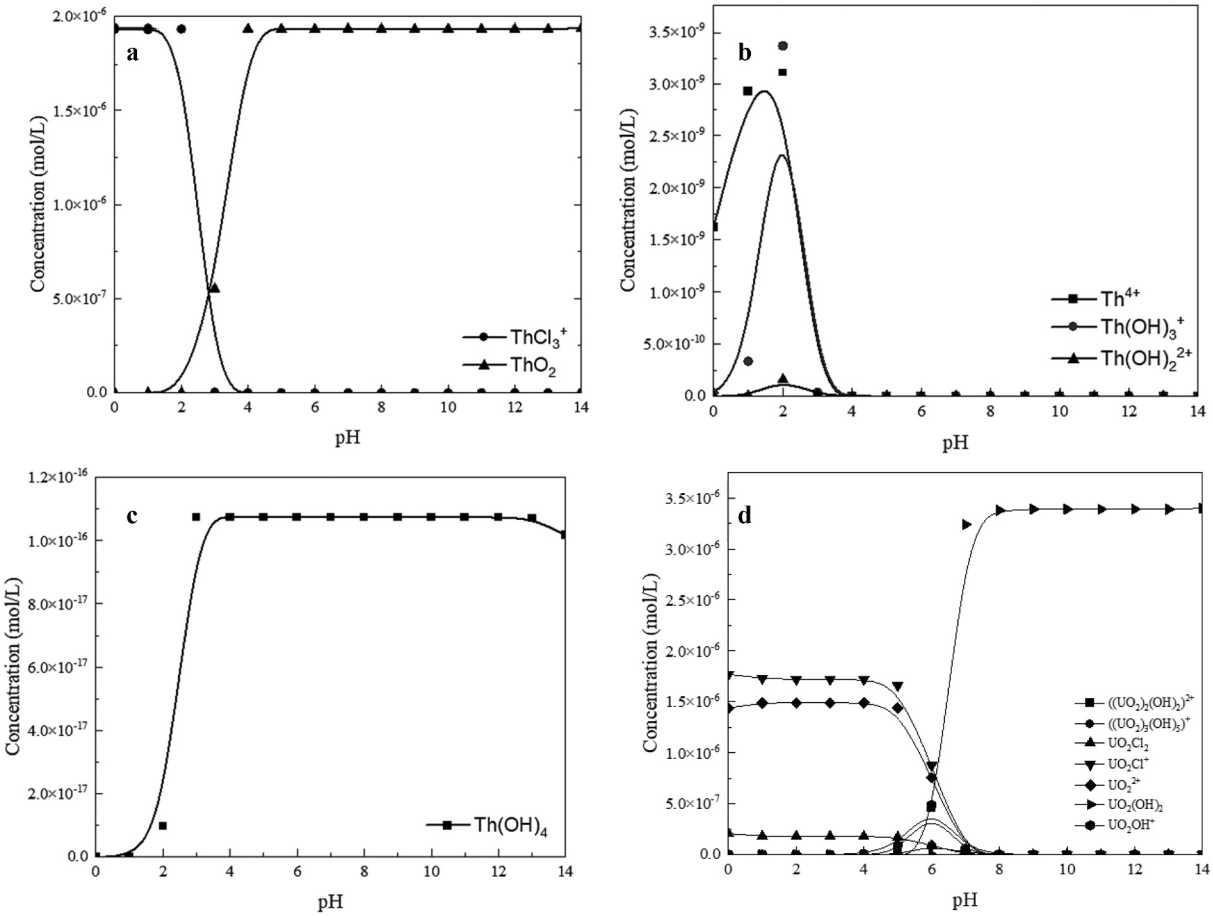

Figure 1. Overall recovery of total rare earths and uranium into the final rare earth product stream. Error bars represent one standard deviation of three replicate tests.

In addition, solvent extraction test results were also analyzed with respect to the distribution ratio, D, and separation factor, β.

$$D = \frac{[C]_{organic}}{[C]_{aqueous}} \tag{8}$$

where $C_{organic}$ denotes the concentration of the element of interest (rare earth elements or uranium) in the organic phase and $C_{aqueous}$ is its concentration in the aqueous phase. If the value of D is greater than 1, it indicates a higher degree of extraction from the aqueous phase into the organic phase. Conversely, a less amount of the element is transferred from the aqueous phase into the organic phase, with the value being less than 1. If D is equal to 1, the amount in each phase is the same with no process selectivity (Giri and Nath 2016). On the other hand, the separation factor β can be described using the following expression:

$$\beta = \frac{D_{REEs}}{D_U} \tag{9}$$

where D_{REEs} and D_U are the distribution ratios of rare earths and uranium, respectively (Giri and Nath 2016). The separation between the two species occurs when the value of β is smaller than 1.

2.3. Process validation studies

After developing an efficient route for separating thorium and uranium from rare earths, additional tests were conducted with a rare earth oxalate sample generated at the same pilot-scale processing plant operated in Kentucky, USA. This sample served as a validation of the developed process. The elemental composition of the rare earth oxalate sample consisted primarily of light rare earths with a total light rare earth concentration of 285.86 mg/g (i. e., lanthanum (66.20 mg/g), cerium (114.80 mg/g), praseodymium (17.78 mg/g), neodymium (72.72 mg/g), samarium (12.46 mg/g), and europium (2.20 mg/g)). The heavy rare earth concentration of the oxalate sample was 15.62 mg/g (i.e. gadolinium (8.56 mg/g), terbium (0.83 mg/g), dysprosium (3.35 mg/g), holmium (0.56 mg/g), erbium (1.32 mg/g), thulium (0.14 mg/g), and ytterbium (0.76 mg/g)). Additionally, scandium and yttrium concentrations were 0.14 and 14.42 mg/g, respectively. As seen, the oxalate sample has a much higher concentration of rare earths, which is around 35%, confirming the successful preconcentration of rare earths at the pilot processing facility. While no uranium was detected, thorium content is 0.12 mg/g, which is significantly higher than the content of the synthetic solution. As for the impurities, calcium, and iron with concentrations of 30.75 and 9.31 mg/g, respectively, were seen.

Upon receiving the sample, it was first subjected to roasting in a muffle furnace at 600°C for 2 hours, which takes advantage of the chemical reactions occurring under high temperatures to enhance the purity of low-grade minerals and improve the efficiency of subsequent processing. After roasting, a residual solid sample of rare earth oxide was obtained, then washed with 0.5 mol/L hydrochloric acid for 15 minutes to remove excess calcium. Representative samples were taken after calcium wash for elemental analysis. Following calcium wash, sample leaching was performed with predetermined test conditions using 6 mol/L hydrochloric acid at 80°C at a solid concentration of 0.5 g/L. Mixing was continued for 24 hours to obtain high dissolution. Next, stage-wise precipitation tests were conducted at room temperature using 50% w/w NaOH to investigate the precipitation characteristics of this new sample as well as to compare and validate previously obtained results from the synthetic solution. When the targeted pH value was reached, the solution was centrifuged for 15 min at 3000 rpm, followed by filtration using 0.45 μm pore-sized filter paper. Afterward, a sample was taken from the filtrate for elemental analysis, and the precipitated solid sample was dried in the oven overnight.

To provide in-depth information, surface morphology and mineralogical identification of the rare earth oxide and precipitated solids were carried out with a Hitachi S-4700 scanning electron microscope (SEM) and a JEOL JEM-2100 transmission electron microscope (TEM) at 200 kV. The electron beam sampling dimension of Energy-dispersive X-ray spectroscopy (EDS) was over ~20 nm under TEM imaging. The SEM analysis was conducted at 5 kV voltage and 12 mm working distance. Prior to SEM analyses, samples were subjected to sputtering using Denton Desk V Sputter and Carbon Coater to prevent charging and improve imaging quality.

3. Results and discussion

3.1. Selective precipitation

At pH 4.8, nearly 100 wt% of thorium precipitated out while 19.3 wt% of rare earth elements and 47.9 wt% of uranium co-precipitated, which generated good separation between thorium and rare earths. However, the overlapping precipitation pH range of uranium (i.e. 5.5–7) and rare earths (i.e. 6.8–8.0) might lead to the co-precipitation of the two by entrapping rare earth elements with uranium or other impurity metals (i.e. iron or aluminum). When the precipitation behaviors of rare earth elements based on different groups (i.e. heavy/light and critical/uncritical rare earths) were further evaluated, a slightly higher heavy rare earth (HREE; Y, Eu, Gd, Tb, Dy, Ho, Er, Tm, Yb, Lu) and critical rare earth (CREE; Y, Nd, Tb, Dy, Eu) precipitation was observed compared to the light (LREE; La, Ce, Pr, Nd, Sm) and uncritical rare earth (UCREE; La, Ce, Pr, Sm, Gd, Ho, Er, Tm, Yb, Lu) group. While heavy rare earth precipitation at pH 4.8 was 20.3%, light rare earth precipitation was 19.5%, critical rare earth and uncritical rare earth precipitations were 19.6 and 19.4%, respectively. This suggests that heavy and critical rare earths tend to precipitate more under these testing conditions than light rare earth elements. Also, this similar phenomenon between heavy and critical rare earth elements is likely due to the overlapping elements in these two groups. A further increase in the solution pH resulted in more rare earth precipitation, and finally, complete precipitation was achieved for rare earth elements when the pH exceeded 8. The observed trend was also seen in the studies conducted by Ponou et al. (2016) and Honaker et al. (2018). Major metal precipitation at the same pH value was approximately 25 wt%, among which iron and aluminum had the most precipitation of 65.6 wt% and 38.5 wt%, respectively.

In this presented study, an in-depth understanding of the precipitation mechanisms was aimed in addition to the experimental testing. Hence, species distribution diagrams were constructed based on a solution system comparable to the laboratory studies for selected rare earth elements, thorium, uranium, iron, and aluminum. The predominance and stability areas of ionic and nonionic species in aqueous solutions are critical to fully understanding the dissolution, leaching, and selective precipitation behavior of different elements. Speciation (species) distribution diagrams are also beneficial to identify major species existing at a particular pH value and provide the ability to predict a change in composition when there is a change in condition.

Thorium's speciation diagrams in the hydrochloric acid medium at 25°C are generated and provided in Figure 2. Due to the low concentrations of some species, separate diagrams were drawn to increase the readability. As seen in Figure 2) the thorium species in the solution are $Th^{4+,}$ $ThCl^{3+}$, $Th(OH)^{3+}$, and $Th(OH)_2{}^{2+}$. Initially, $ThCl^{3+}$ is formed due to the reaction between Cl^- and Th^{4+} ions. In Figure 2), $ThCl^{3+}$ and ThO_2 display opposite behaviors. As the concentration of $ThCl^{3+}$ decreases, the formation of ThO_2 becomes apparent. However, when an alkaline reagent (i.e. NaOH) is introduced to the solution, the reaction is reversed, releasing Cl^- ions back and freeing Th^{4+} ions to react with OH^-. It explains the increasing concentration of Th^{4+} between pH 0 and 2 (Figure 2)). The decrease observed later in Th^{4+} concentration is due to the complexes formed with the OH^- ions liberated from NaOH, which also initiates the precipitation. Meanwhile, a substantial increase of thorium hydroxide ($Th(OH)_4$) is seen (Figure 2)) with an elevation in the solution pH. However, due to the unstable nature of thorium hydroxide, it slowly transforms into thorium dioxide (ThO_2), a partially microcrystalline hydrous oxide, as shown in reaction 8 (Brookins 1988; Neck and Kim 2001). The concentration of $Th(OH)_4$ reaches a steady level at a pH value of 4. Similarly, ThO_2 formation becomes stable at a pH value slightly higher than 4, the pH region in which thorium precipitation is assumed to be completed. A further increase in the pH does not change the concentrations of any species.

$$ThO_2.H_2O + H_2O \rightarrow Th(OH)_{4(aq)} \tag{10}$$

Starting precipitation pH values were also calculated for thorium, uranium, rare earth elements, iron, and aluminum. Precipitation starts when the saturation index (I) reaches zero, indicating equilibrium between the ion activity products (IAP) and solubility product (K). The ion activity products and calculated starting precipitation pH of the elements were stated in the captions of the species distribution diagrams. According

to the calculations, starting precipitation pH for ThO_2 is 3, which is in agreement with the species distribution diagram. Thorium chloride starts to dissociate, the freed thorium ions begin to react with hydroxide ions, and finally, the formation of ThO_2 starts at pH 3 and levels off at around pH 5. In the literature, the precipitation pH range of thorium is reported as pH 2.5 to 5.5 (Zhu, Pranolo and Cheng 2015), which correlates with the results obtained from saturation indices and species distribution diagrams. However, even though a solid formation was observed at pH 3, the particles did not settle during the experiments, and no separation between solid and liquid phases was achieved. Further increase in the pH resulted in an enhanced separation between the aqueous and solid phases. It also resulted in more precipitation, and complete thorium separation was achieved at pH 4.8. Thermodynamic studies were also performed following the precipitation reaction. The Gibbs free energy change of the reaction is −125.52 kJ/mol at the standard state conditions (1 atm and 25°C). The negative value of ΔG indicates the precipitation of thorium dioxide is thermodynamically favorable, while an enthalpy value of −114 kJ/mol further supports and suggests an exothermic reaction. According to reaction (7), the entropy

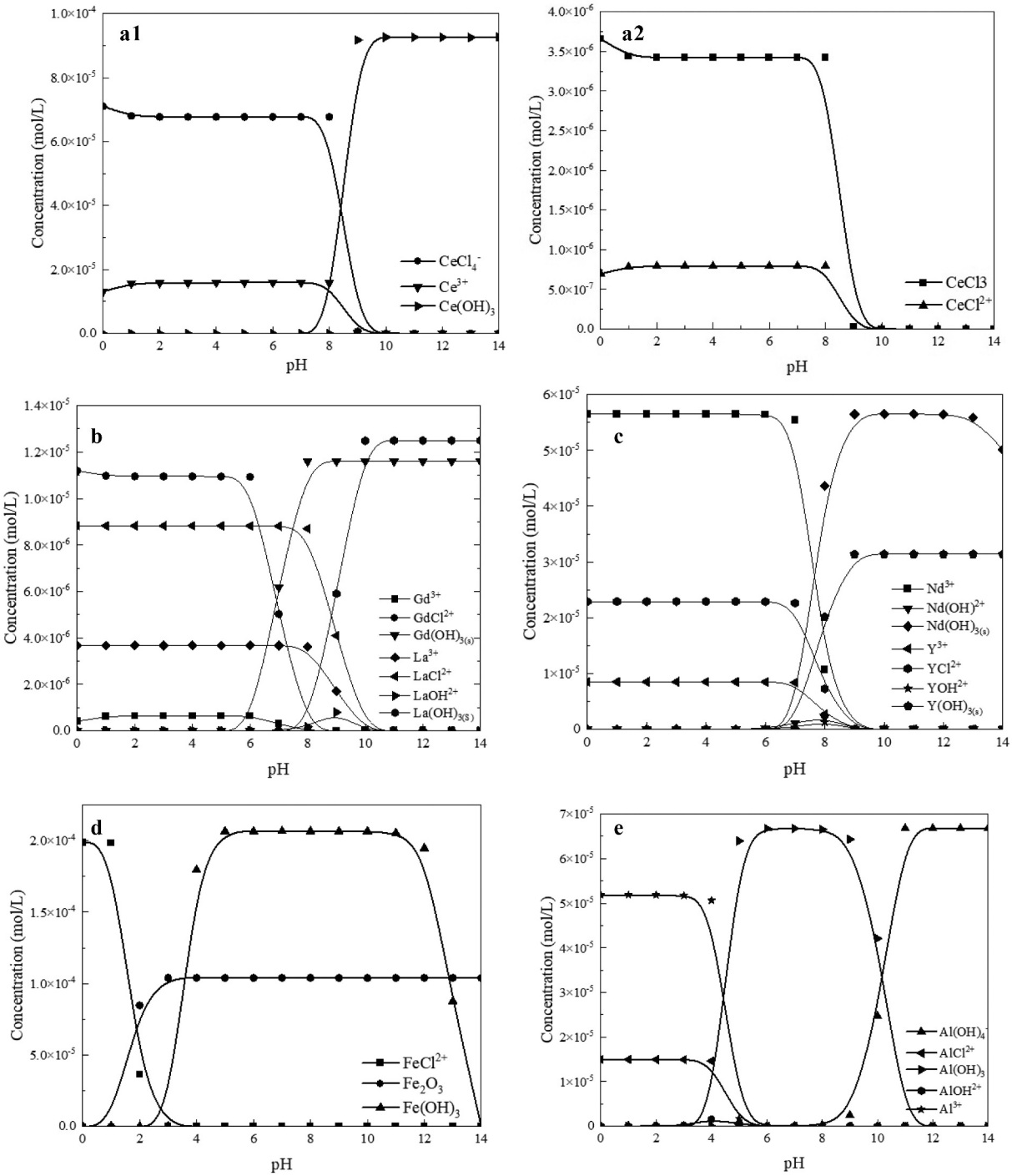

Figure 2. Species distribution diagrams of (A), (B), (C) Th-HCl system (log IAP = 1.77 and starting precipitation pH = 3), (D) U-HCl system (log IAP = 5.62 and starting precipitation pH = 7.4).

value of thorium precipitation is found to be 39 J. $mol^{-1}.K^{-1}$. Overall, the conclusions reached in this study were in support of the literature from both experimental and fundamental points of view (Felmy, Rai and Mason 1991; Zhu, Pranolo and Cheng 2015).

On the other hand, uranium can be seen in many forms, such as U (III, IV, V, VI). Among them, U (IV and VI) are the most common states (Monji, Ghoulipour and Mallah 2016). The speciation of uranium in chloride media is given in Figure 2). Uranium initially exists in the solution with its 6^+ oxidation state. According to the literature data, the precipitation of uranium starts at a pH value approaching 6 (Zhu, Pranolo and Cheng 2015), which means the solubility of the ions decreases, and the tendency to create insoluble complexes increases. At lower pH values conditions (pH<5), uranium exists as UO_2^{2+}, which is well correlated with the results obtained in this study (Langmuir 1978; Monji, Ghoulipour and Mallah 2016). As seen in Figure 2), the predominant species are UO_2^{2+} and UO_2Cl^+ at lower pH values, and their concentration starts changing when pH exceeds 4 and then decreases sharply at pH 5. As the concentrations of UO_2Cl_2, UO_2^{2+}, and UO_2Cl^+ are lessening, the uranyl hydroxide ($UO_2(OH)_2$) starts to be formed. Supporting trends were also observed in Figure 2), where ionic species, especially $UO_2(OH)^+$, $(UO_2)_2(OH)_2^{+2}$, $(UO_2)3(OH)_2^+$ display a dominant behavior and have their peak at pH 6. Due to the complexation occurring between uranium and hydroxide ions, the concentrations of $UO_2(OH)^+$, $(UO_2)_2(OH)_2^{+2}$, $(UO_2)3(OH)_2^+$ first increase and reach their respective maximum levels and then decrease as the solution pH increases (pH>6). Similar findings were also seen in Orabi's study (2013). The ion activity of $UO_2(OH)_2$ gradually increased from −4.24 to 5.62 as pH increased from 1 to 7.4, and the system reached equilibrium at pH 7.4 when uranium precipitation started. It is also the pH value where $UO_2(OH)_2$ line levels off. The early start of precipitation seen in the species distribution diagram may attribute to the formation of $UO_2(OH)_{2(aq)}$, as it would be formed first due to a smaller solubility constant (i.e. −12.15). Similar to thorium, the precipitation of $UO_2(OH)_2$ (reaction 11) has been spontaneous and exothermic with ΔG and ΔH values of −65.69 kJ/mol and −56.76 kJ/mol, separately, at the standard state conditions. The entropy of the reaction was calculated to be 30 $J.mol^{-1}.K^{-1}$.

$$UO_{2(aq)}^{2+} + 2OH_{(aq)}^{-} \rightarrow UO_2(OH)_{2(s)} \quad (11)$$

The species distribution diagrams of selected rare earth elements are shown in Figure 3. Five rare earth elements (i.e. cerium, neodymium, gadolinium, lanthanum, and yttrium) were selected based on their dominant concentrations in the feedstock solution and to represent different rare earth groups (i.e. heavy, light, critical, and uncritical rare earth elements). It is known that most rare earth elements existed in the synthetic solution as $REEs^{3+}$. However, they may also have divalent or tetravalent states, but these states of rare earths are not stable (Thakur 2000). Rare earths become less soluble with increasing pH, and thermodynamically stable rare earth hydroxides can be obtained by treating aqueous solutions with a basic chemical reagent. Rare earths' resistance to the base and solubility decreases from light rare earths toward heavy rare earths, with lanthanum being the most alkali and soluble, having the highest solubility constant. Table 1 confirms that lanthanum hydroxide has a solubility constant (log K) of 20.29. It is then followed by cerium, neodymium, yttrium, and gadolinium with solubility products (log K) of 19.89, 18.09, 17.49, and 15.09, separately (Table 1). On the other hand, cerium (IV) and scandium exhibit the opposite behavior (Stevenson and Nervik 1961). The species distribution diagrams of lanthanum and cerium (Figures 2A1 and D) support the above statement.

As seen in the diagrams, the precipitation behavior of rare earths is alike. REE^{3+}, $REECl^{2+}$, and $REE(OH)^{2+}$ are the common species observed for all studied elements. Typically, free rare-earth ions, REE^{3+}, and $REECl^{2+}$ ions dominate at lower pH values. $REE(OH)^{2+}$ starts to appear when precipitation reactions occur. The conclusions reached here agree with Agarwal and his coworkers' (2018) study, where the aqueous behavior of yttrium was investigated in various acidic media. However, two additional chloride species, $CeCl_4^-$ and $CeCl_3$, were also observed for cerium. On the other hand, the neodymium-HCl system contains a different hydroxide species, $Nd_2(OH)_2^{4+}$. Even though their behavior is generally uniform, species diagrams for gadolinium, lanthanum, and cerium illustrate slight differences. While neodymium (Figure 3) and yttrium (Figure 3) hydroxides start to be formed at pH 6, lanthanum (Figure 3) hydroxide and cerium (2A1 and A2) hydroxide formation initiate later, at pH 7. On the other hand, gadolinium starts to be formed even at an earlier pH value, slightly higher than pH 5 (Figure 3). These observations also explain the minor difference in precipitation behavior of heavy, light, critical, and uncritical rare earth elements. When equilibrium studies further continued, it revealed that the actual cerium precipitation starts at pH 8.6, where $CeCl_4^-$ meets $Ce(OH)_3$. First, the concentrations of $CeCl_3$ and $CeCl_{2+}$ are lessening, then the lines representing $CeCl_4^-$ and $Ce(OH)_3$ cross each other (Figures 2A1 and A2). For neodymium, precipitation starts at pH 7.8, where Nd^{3+} and $Nd(OH)_3$ intercept in Figure 3). As for gadolinium, pH 7 is the equilibrium point at which the Gd^{3+} line coincides with the $Gd(OH)_3$ line (Figure 3). Lanthanum precipitation starts at the latest, i.e. pH 8.8. The transition of La^{3+} ions into $La(OH)_3$ can also be seen from the curve of $La(OH)^{2+}$ in Figure 3. In addition, yttrium's precipitation starts at pH 8, which displays a similar characteristic as lanthanum. The difference between the actual starting precipitation pH values and the pH values where $REE(OH)_3$ formation lines start is due to the changes occurring within the species. Instead of directly producing rare earth hydroxides, the species undergo dissociation or reaction, and then finally, the rare earth hydroxides are formed. Due to their similar characteristics, the thermodynamic values for the studied rare earth elements were found to be considerably close to each other. The Gibbs free energy change of the studied rare earth elements varied between −124.6 to −173.5 kJ/mol. The enthalpy of the reactions changed between −19.7 to −59.3 kJ/mol, which all indicated an exothermic and spontaneous precipitation reaction for rare earth

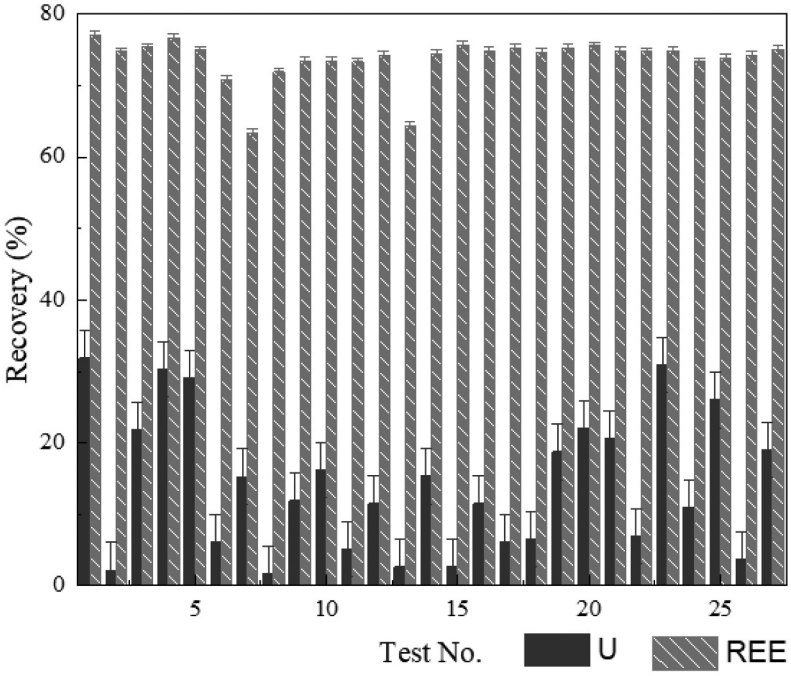

Test	H_2SO_4 (mol/L)	TBP (v%)	pH	O/A
1		30	3.5	1
2		40	4.5	1
3		50	3.5	1
4		40	2.5	1
5		30	2.5	2
6		30	4.5	2
7		30	3.5	3
8	1	50	3.5	3
9		40	3.5	2
10		50	2.5	2
11		40	3.5	2
12		40	3.5	2
13		40	4.5	3
14		40	2.5	3
15		50	4.5	2
16		40	4.5	2
17		50	3.5	2
18	0.5	40	3.5	3
19		40	3.5	1
20		30	3.5	2
21		40	2.5	2
22		50	3.5	2
23		30	3.5	2
24	2	40	4.5	2
25		40	3.5	1
26		40	3.5	3
27		40	2.5	2

Figure 3. Species distribution diagrams of REEs-HCl system. (A1 & A2) Cerium (log IAP = 19.89 and starting precipitation pH = 8.6), (B) Neodymium (log IAP = 18.09 and starting precipitation pH = 7.8), Yttrium (log IAP = 17.49 and starting precipitation pH = 8.0), (C) Gadolinium (log IAP = 15.09 and starting precipitation pH = 7.0), Lanthanum (log IAP = 20.29 and starting precipitation pH = 8.8), (D) Iron (log $IAP_{(Fe2O3)}$ = 1.42 and starting precipitation pH = 2.8, log$IAP_{(Fe(OH)3)}$ = 38.55 and starting precipitation pH = 3.0), (E) Aluminum (log IAP = 7.74 and starting precipitation pH = 4.8).

elements. Additionally, these thermodynamic findings imply that heavy rare earth elements tend to precipitate as opposed to light elements as a more negative ΔG value is obtained for heavy rare earths: gadolinium (−143.6 kJ/mol) and yttrium (−173.5 kJ/mol) compared to cerium (−130.5 kJ/mol), neodymium (−136.9 kJ/mol), and lanthanum (−124.6 kJ/mol), which confirms the precipitation data mentioned above.

$$REEs^{3+}_{(aq)} + 3OH^{-}_{(aq)} \rightarrow REEs(OH)_{3(s)} \quad (12)$$

The speciation of iron (Figure 3) and aluminum (Figure 3) in the chloride media were also investigated. In the synthetic feedstock solution, iron exists in its trivalent oxidation state, Fe^{3+}. Due to the nature of the synthetic solution's medium, iron (III) chloride ($FeCl_3$) is also present in the solution, and its concentration starts to decrease at pH 3, the same pH value as Fe^{3+} decreasing. While the concentrations of Fe^{3+} and $FeCl_3$ reduce, iron hydroxide ($Fe(OH)_3$) formation starts around pH 3, which supports the calculated starting precipitation pH. The formation of $Fe(OH)_3$ continues until pH 5 and shows a stable behavior between pH 5 to 11; however, when the pH reaches 12, the formation of $Fe(OH)_3$ inverses. The presence of hematite is also observed, starting early in the solution (pH 2.8) and reaching a constant concentration level at pH 3. Iron precipitation is thermodynamically stable with a corresponding ΔG value of −317.13 kJ/mol and an ΔH value of −229.43 kJ/mol. Generally, the formation of $Al(OH)_3$ starts to be seen at a pH value of 5 (Balintova and Petrilakova 2011). In this study, agreed with the literature, the starting precipitation pH for gibbsite was calculated as 4.8. As chloride species are liberated, Al^{3+} gradually transforms into hydroxide forms. The concentrations of $AlCl^{2+}$ and Al^{3+} decrease as the pH increases, and the Al^{3+} line intercepts with $Al(OH)_3$ at around pH 5. The formation of $Al(OH)_3$ stays constant between pH 6 and 10, and then the reaction changes resulting in a reduction in the concentration with a further increase in the pH. As the concentration of $Al(OH)_3$ reduces, $Al(OH)_4^-$ becomes the dominant species. Like iron, the aluminum precipitation mechanism is thermodynamically favorable, with a standard energy change value of −540.03 kJ/mol. Moreover, the enthalpy change, −545.53 kJ/mol, suggests an exothermic reaction.

$$2Fe^{3+}_{(aq)} + 3H_2O - 6H^{+} \rightarrow Fe_2O_{3(s)} \quad (13)$$

$$Fe^{3+}_{(aq)} + 3OH^{-}_{(aq)} \rightarrow Fe(OH)_{3(s)} \quad (14)$$

$$Al^{3+}_{(aq)} + 3OH^{-}_{(aq)} \rightarrow Al(OH)_{3(s)} \quad (15)$$

3.2. Solvent extraction

Due to the close precipitation pH ranges and the similarities in the ionic radii of uranium and rare earth elements, the separation between these two required additional treatment. As a result of the 27 previously designed tests, the rare earth recovery obtained from solely the solvent extraction circuit varied from 80.2 wt% to 97.6 wt%, while the corresponding uranium recovery changed from 3.4 to 62.5 wt%. On the other hand, considering the amount of rare earths and uranium previously precipitated as solid forms, the overall recovery of rare earths and uranium varied from 64.7 wt% to 78.7 wt% and 1.8 wt% to 32.5 wt%, respectively (Figure 1). Among all 27 tests, the lowest uranium recovery, 3.4 wt%, into the rare earth

product stream was produced by Test 8 (i.e. 50 v% TBP, pH 3.5, O/A ratio 3, 1 mol/L H_2SO_4) with a corresponding rare earth recovery of 91.0 wt%. On the other hand, the highest rare earth recovery, 97.6 wt%, into the final product stream was generated by Test 1 when 30 v% TBP was used at an O/A ratio of 1 with 1 mol/L H_2SO_4 at a solution pH of 3.5. However, the operating conditions of Test 1 resulted in a considerably higher uranium recovery of 62.5 wt%. The amount of rare earths and uranium lost into the organic phase is low. For example, for Test 8, no uranium was recovered into the organic stream based solely on solvent extraction. Under the same conditions, 3.4% of uranium was reported to the rare earth product stream, and the remaining uranium was reported to the uranium product stream. In addition, the amount of rare earths reporting to the organic stream was negligible (<1%) for most of the tests, and the highest recovery of rare earths into the organic stream was seen as 5.9%.

Chemical reactions occurring during extraction and stripping stages are shown in reactions (16)-(18). The extraction ability of tributyl phosphate is attributed to the phosphoryl group, which forms solvates with the metal ions in the solution (Giri and Nath 2016). The extraction of rare earths increases proportionally to the atomic number (Peiro and Mendez 2013), and the extraction of uranium and rare earths in TBP-HCl follows the order of U> REEs (Qi 2018). Distribution ratios were also calculated for total rare earths and uranium during each extraction step. Although the distribution ratio is not necessarily related to the extraction efficiency, it is an indicator of the necessity of multistage extraction. For rare earth elements, D_1, representing the element concentration ratio of organic to aqueous phases during the first extraction, changed between 0 to 0.035. Generally, a decrease in the second distribution ratio (D_2) was observed for rare earths. This may occur due to the completion of extraction during the first stage. However, there are a few exceptions for which the second step enhanced the extraction of rare earths. For instance, as a result of Test 7 (i.e. 30% TBP, pH 3.5, O/A ratio 3, 1 mol/L H_2SO_4) and Test 16 (i.e. 40% TBP, pH 4.5, O/A ratio 2, 0.5 mol/L H_2SO_4), an increase in the rare earth element distribution in the organic phase was observed. Overall, the distribution ratios (D_1 and D_2) for rare earths are low, with most values less than 0.03. A similar trend was observed for uranium, although this time, the effect of the second extraction step is more profound. The distribution ratio of uranium under the best-operating conditions (Test 8; 50 v% TBP, pH 3.5, O/A 3, 1 mol/L H_2SO_4) changed from 0.84 (D_1) to 2 (D_2), which resulted in the lowest uranium recovery into the final rare earth product stream. The separation factor between REEs/U was also calculated. The separation factor is a good measurement of the extractant's separation ability. The data indicated the effect of two-stage extraction on selectively removing uranium from rare earths based on the decreasing separation factor at the end of the second extraction step. The separation factor for the first extraction step varied from 0 to 0.22, whereas the second extraction step reduced this range from 0 to 0.10.

$$UO_2Cl_2 + 2TBP \rightarrow UO_2Cl_2.2TBP \quad (16)$$

$$REECl_3 + 3TBP \rightarrow REECl_3.3TBP \quad (17)$$

$$3UO_2Cl_2.2TBP + H_2SO_4 \rightarrow UO_2SO_4.3H_2O + 2TBP + 6Cl^- \quad (18)$$

Upon completing the solvent extraction tests, the statistical analyses of the results were performed using the Design-Expert software. A mathematical model was developed to predict uranium recovery. It can be seen from the model that all variables except the stripping agent concentration had a significant impact on uranium recovery.

$$\begin{aligned} UraniumRec. = {} & +18.64 - 13.06 * A - 15.41 * B \\ & + 1.99 * C - 14.02 * D + 4.75 * AB - 3.90 * AC - 1.74 * AD \\ & + 0.54 * BC + 7.55 * BD - 4.92 * CD + 8.24 * A^2 + 2.25 * B^2 \\ & + 6.29 * C^2 + 4.54 * D^2 (R^2 = 0.8731) \end{aligned} \quad (19)$$

where A, B, C, and D correspond to the extractant concentration, feed solution pH, strippant concentration, and O/A ratio, respectively.

It was observed from the experimental test results that an increase in the operational parameters produces a lower uranium recovery into the rare earth product stream. However, when the interacting effect of the model terms was further analyzed, reducing uranium recovery does not depend solely on a single parameter. A simultaneous increase in the extractant concentration, O/A phase ratio, and solution pH generates the best separation performance. One of the highest uranium recovery values of 57.2% was observed when the feed solution pH and extractant concentrations were 2.5 and 30% by volume, respectively. A gradual increase in the pH and extractant concentration lowered uranium recovery. The lowest uranium recovery (i.e. 3.4%) into the rare earth product stream was obtained at a pH value of 3.5 with 50% TBP by volume. These findings prove that the feed solution pH and the extractant concentration are the two critical factors impacting uranium recovery. The uranium recovery into the final product stream decreased with an increase in both extractant concentration and O/A ratio. The highest uranium recovery of 62.5% was achieved with the lowest extractant concentration (30% TBP by volume) and O/A phase ratio of 1. It can be concluded that a low O/A phase ratio may not be sufficient to extract uranium ions from the aqueous phase for the separation purpose. Therefore, an increase in the O/A ratio results in an improved separation. Additionally, a high O/A ratio and pH produced noticeably enhanced separation results. Similar findings were also obtained in Jorjani and Shabazi's study (2012). As indicated and statistically supported by the model, pH is an influential parameter, and the best result was obtained at a pH value of 3.5. Moreover, a lower uranium recovery observed with increased solution pH suggests that the higher pH favors creating more stable uranium-TBP complexes. The concentration of sulfuric acid tested in the study did not significantly impact the separation results. The lowest uranium recovery was generated using 1 mol/L sulfuric acid. Even though an increase in the

concentration of stripping agent from 0.5 mol/L to 1 mol/L lowered the uranium recovery, a further boost from 1 mol/L to 2 mol/L had a minimum impact on uranium recovery. This indicates that 1 mol/L H_2SO_4 solution was sufficient to break the uranium-TBP complex and strip uranium into the aqueous phase.

Statistical analysis was also performed for the prediction of total rare earth recovery; however, the analysis indicated that the model is not significant. Nonetheless, the model's insignificance is consistent with the experimental findings showing no substantial change in the recovery of total rare earths under all tested conditions. It also supports the study's objective to investigate the effect of different operating variables on uranium recovery instead of rare earth recovery. Therefore, the input operating variables had a minimum impact on the recovery of rare earths compared to uranium. The finding confirms the selectivity of the experimental design.

3.3. Process validation studies

Stage-wise precipitation test results obtained with the rare earth oxalate produced at the pilot-scale facility were aligned with the experimental results presented above using the synthetic solution. The developed approach was thus validated. At a pH value of 4.6, approximately 95% of thorium precipitated along with 11.4% rare earth element co-precipitation. A continuous increase in solution pH led to a further precipitation of rare earths, reaching completion at pH 9.5. While very little change (i.e. by 4%) in the precipitation of rare earths was observed from pH 4.6 to 5.5, a significant jump was seen between pH 5.5 (i.e. 15.4% precipitation) to pH 7 (i.e. 36.2% precipitation). Another, and the most significant, incremental increase in the precipitation of rare earths was seen between pH 7.5 (i.e. 37% precipitation) and pH 8 (i.e. 74.8% precipitation), accounting for an additional 37.8% of total rare earth precipitation.

SEM was utilized to compare the particle surface morphologies before and after precipitation. The microscopic images of the rare earth oxide (Figure 4) indicated a rough surface of rare earth oxide consisting of various agglomerated particles. A close look at the solid surface further shows the presence of layered structures, rods, and irregular-shaped particles being sintered together. Moreover, tiny nano-sized particles are also deposited on the solid surface. The fuzzy edges of several particles indicate the decomposition and sintering the sample went through during the previous calcination treatment. On the contrary, the SEM images of solids obtained via precipitation (Figure 4) had a very smooth surface with clearly identified cubic-shaped particles resembling the crystal structure of salt (NaCl). It is due to the reaction occurring between sodium hydroxide and the solution medium, hydrochloride acid.

Characterization studies further continued with TEM analyses to provide in-depth information. TEM images of the rare earth oxide feed sample are given in Figure 4). The polycrystalline rods with a length of up to ~ 2 μm were found to be enriched with rare earth elements, such as lanthanum, cerium, and neodymium. The highest enrichment of lanthanum was detected in Figure 4) in region 1, with a concentration of 8.2 wt%. Other lanthanum enrichments were seen in regions 7 (4 wt%), 8 (6.5 wt %), 9 (3.8 wt%), and 10 (4.2 wt%) in Figure 4). Cerium and neodymium were detected more than lanthanum, and both were seen in regions 1, 3, 5, 7–10 in varying amounts. The highest cerium observed was 21.4 wt% in Figure 4), region 1, followed by regions 5 and 3 with a content of 20.3 wt% and 19.8 wt%, separately. The remaining regions (7–10) contained around 11 to 16.5 wt% of cerium. On the other hand, the highest neodymium of 10.6 wt% was seen in region 5, followed by 10.3 wt% in region 1 and 9.5 wt% in region 3. The rest of the neodymium detection varied between 5.1 wt% to 8.2 wt%. Overall, these three elements (i.e. lanthanum, cerium, and neodymium) were identified as the most highly enriched rare earths in the oxide sample, with a content varying from 3.8 to 21.4 wt%. Although it was not much, yttrium and gadolinium were also identified in several local regions. 2.8 wt% yttrium was seen in region 7 in Figure 4), while regions 9 and 10 both contained 1.8 wt% yttrium. Gadolinium of 0.7 wt% was only detected in region 10. All these suggest the successful enrichment of rare earths from coarse coal refuse at the pilot-scale processing facility. Moreover, around 7 wt% and 6 wt% cobalt were detected in regions 7 and 1, respectively, indicating the co-extraction of rare earth elements and cobalt and the potential to recover cobalt as another critical mineral product. In addition, impurity metals of iron and aluminum co-existed with rare-earth elements, while silicon was detected in regions 9 and 10. 3.4 wt% of aluminum was found only in region 9. On the contrary, iron enrichments were seen in several regions where region 6 contained 100 wt% iron. Similarly, high calcium content is seen in regions 2 and 4, with a corresponding concentration of 100% and 30.2 wt%, respectively, suggesting the need for downstream calcium wash. Successful removal of those contamination elements will substantially increase the rare earth grade further.

TEM analyses of the solids precipitated at pH 4.6 are seen in Figure 4). The snow-flake-like crystals are enriched with sodium chloride (NaCl), supporting the SEM image analysis results. A small amount of rare earth elements like cerium (0.2 wt% to 9.2 wt%) and neodymium (0.8 wt% to 3.1 wt%) were also seen in the precipitated solid, especially in regions 2, 10, 11, and 12 in Figure 4). The highest cerium detection, 9.2 wt%, was in region 10, followed by 7.7 wt% in region 2. Likewise, the highest neodymium was observed in region 10, with a neodymium content of 3.1 wt%. Lanthanum was also sparsely identified in some local regions, region 2 containing 2.8 wt% of lanthanum, and region 10 containing 4 wt% of lanthanum. This aligns with the precipitation data discussed earlier that around 11.4% of rare earths were lost due to the co-precipitation with thorium. However, thorium was not detected in the precipitated solids, which is likely due to its low concentrations compared to other elements. Except for iron, no other metals were detected in this solid sample. Compared to the feedstock (rare earth oxide), the precipitated solid contained less iron. Although it was detected in almost every region in Figure 4), the amount detected was low, varying between 0.4 wt% to 14.4 wt%, in which region 5 has the highest and region 10 has the lowest content. Besides, no calcium was detected within the solid (except for region 2 (< 1 wt%)), suggesting the efficiency of calcium wash prior to

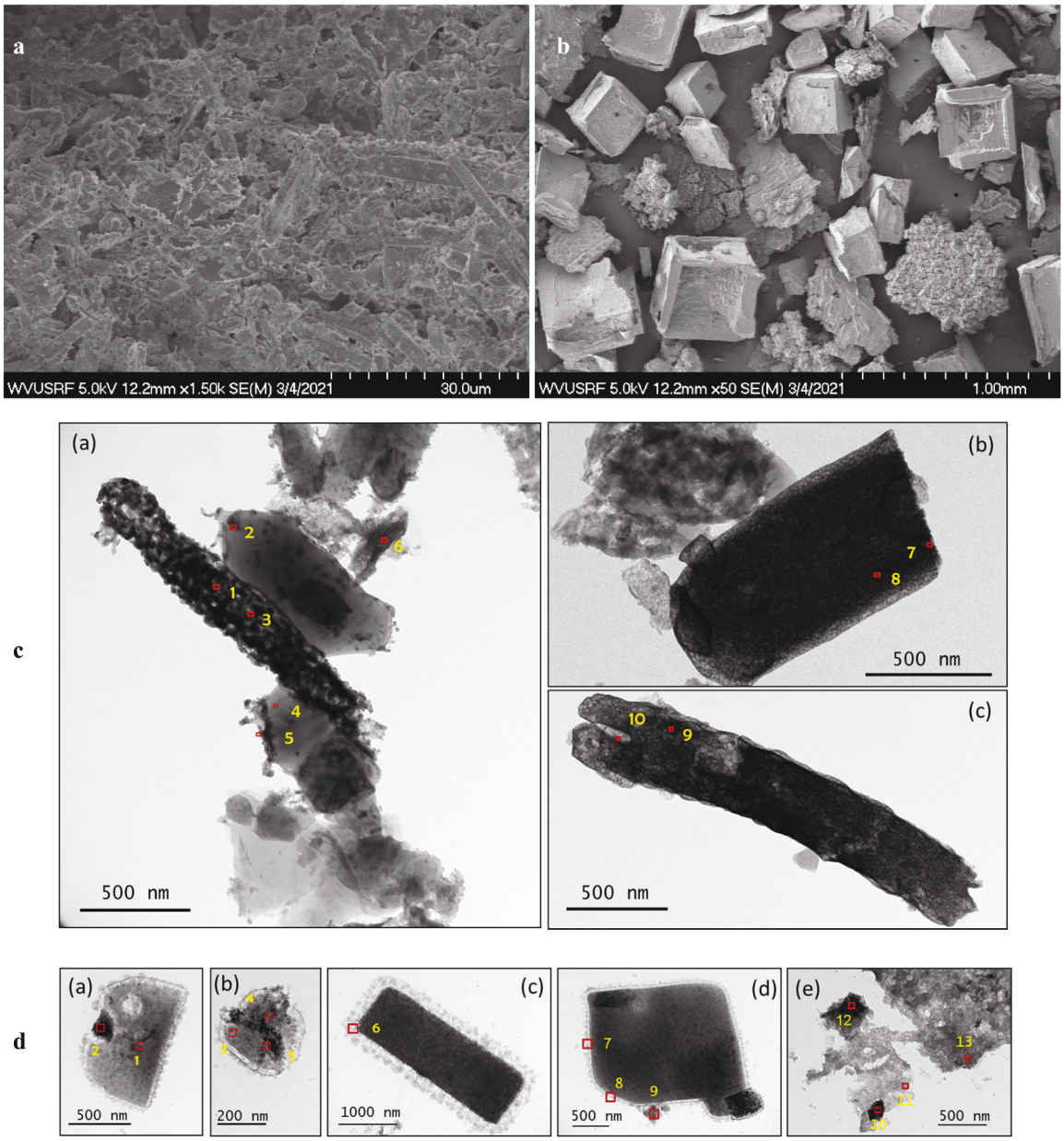

Figure 4. SEM images of (A) the rare earth oxide feed sample, (B) precipitated solids at pH 4.6, (C) TEM images of the rare earth oxide feed sample; rod structures with darker contrast in (a-c) are enriched with rare earth elements, (D) TEM images of solids precipitated at pH 4.6. (a-d), NaCl crystals with a trace amount of Ce and Fe; (e), NaCl flakes that are enriched with Ce, Nd, and La.

selective precipitation. In addition to the elements presented above, sodium, chloride, and oxygen were detected in every region.

2.4 Conceptual process flowsheet development

Based on the studies conducted on both synthetic solution and the rare earth oxalate generated at the pilot-scale plant, a conceptual process flowsheet was developed. It aims to shed light on the process that can be potentially adapted to produce high purity rare earth products from coal and coal by-products without the contamination of thorium and uranium (Figure 5). The proposed process flowsheet is comprised of five main unit operations. As seen, the unit operations contained in the flowsheet include (1) feedstock leaching, (2) selective thorium removal by precipitation, (3) uranium removal by solvent extraction, (4) rare earth oxalate precipitation, and (5) roasting for rare earth oxide production.

Following the developed flowsheet and proper sample preparation such as crushing and grinding or physical pre-concentration, coal and coal by-products with suitable feedstock specifications are introduced to the leaching tank where acid dissolution at an elevated temperature (e.g. 80°C) is achieved. After sufficient retention time in the leaching tank, typically 2 hrs, the pregnant leach solution is subjected to filtration to remove undissolved residues. The loaded leach solution is transferred to the second unit operation, where selective thorium removal is targeted via one-stage precipitation. It is recommended to keep the solution pH below 5

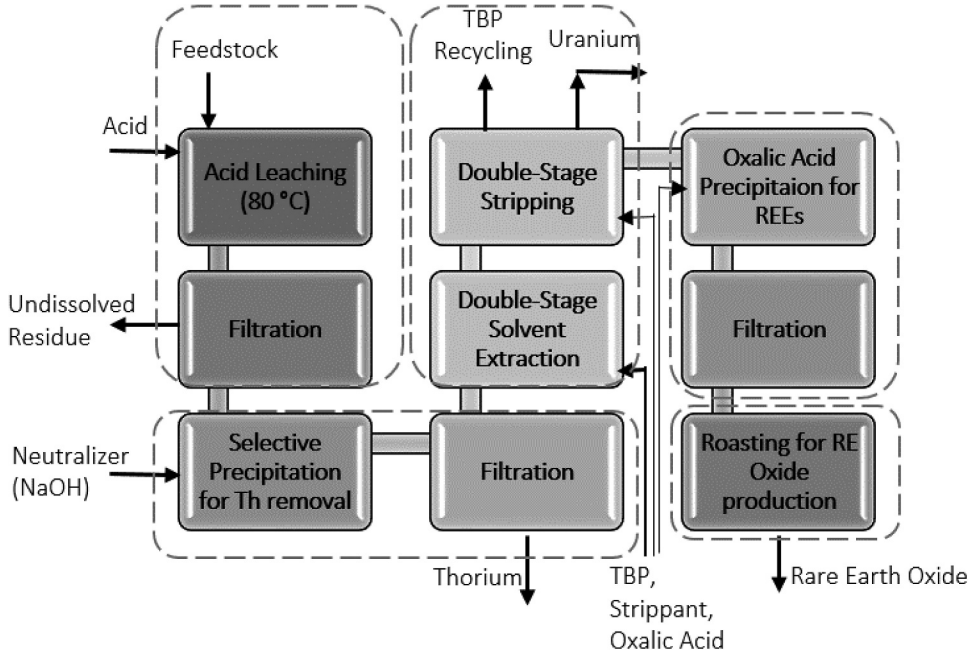

Figure 5. Conceptual process flowsheet developed to produce rare earth elements and remove thorium and uranium from coal and coal by-products.

to prevent excessive loss of rare earth elements due to their entrapment in thorium, iron, or aluminum precipitates. If a significant loss is observed due to the dominancy of impurity metals and consequent surface adsorption, a re-dissolution-re-precipitation route can be followed to recover the lost rare earths (Zhang and Honaker 2019). After the targeted pH is reached, the solution is subjected to secondary filtration. Thorium is thus separated from the solution and sent to the tailing pond. The materials in this tailing pond can be utilized as mine backfilling since the concentration of thorium will be diluted by mixing it with other residues (Findeib and Schaffer 2017).

On the other hand, the remaining filtrate is subsequently pumped to solvent extraction mixer-settlers to further separate uranium from rare earths. In the case of substantial contamination of the organic phase by higher concentration ions, scrubbing can be applied using a mild acid solution to purify the organic phase for reuse. After solvent extraction, the loaded aqueous phase, i.e. uranium product stream, is sent to a pond, where it will be neutralized. The radioactivity level of the thorium and uranium ponds must be monitored regularly to meet environmental compliance. On the other hand, the used extractant is pumped to the recycling unit for further purification and reuse. To recycle the organic extractant, sodium carbonate, ammonium nitrate solution, and deionized hot water can be used to remove undesirable elements, such as calcium, iron, magnesium, and phosphorus (Choppin and Khankhasayev 1998; IAEA 2000).

In the meantime, the rare earth-containing aqueous stream is subjected to oxalic acid precipitation followed by filtration and roasting to eventually produce pure rare earth oxide products. If further purification is required, it can be achieved by dissolving the precipitated rare earth oxalate solid in a carbonate-containing solution (i.e. Na_2CO_3 and $NaHCO_3$), where the elements other than rare earths will create a soluble complex (Amer et al. 2013; Yang et al. 2019).

4. Conclusions

As the world's coal consumption increases, it will continue generating tremendous tailings in various forms, such as coarse and fine refuse, bottom ash, fly ash, slag, etc. Therefore, the utilization of coal processing products presents a significant potential in achieving sustainable mining and a circular economy by turning coal wastes into the feedstock of rare earth. Nonetheless, the association of thorium and uranium with rare earth minerals, regardless of primary or secondary sources, is a significant issue that requires continuous attention and monitoring. This study explored the separation of thorium and uranium from a rare earth-containing solution generated from an unconventional feedstock, i.e. coarse coal refuse. A conceptual process flowsheet was developed based on the study findings. Separation was accomplished with an experimental route combined with selective precipitation and solvent extraction. In addition to laboratory studies, the fundamental aspect of applied methods was also investigated. Equilibrium and thermodynamic studies were performed to explore the precipitation behaviors and extraction mechanisms of various elements. The distribution ratio and separation factor were determined for solvent extraction to evaluate uranium separation under different operating conditions. The conclusions reached from this study include:

(1) Experimental data obtained from selective precipitation and solvent extraction tests indicated that the former method is more selective toward thorium separation. At the same time, the latter had a superior performance for uranium removal from rare earth elements.
(2) At a solution pH of 4.8, nearly all thorium precipitated out while approximately 19.3 wt% of rare earth elements and 47.9 wt% of uranium co-precipitated. The precipitation reactions were all spontaneous and exothermic for the elements studied based on calculated

Gibbs energy and enthalpy values. All precipitation reactions were thermodynamically favorable at the standard state operating conditions.

(3) Due to the overlapping precipitation pH ranges of uranium and rare earth elements, a further separation technique, solvent extraction, was utilized. The recovery of rare earths into the rare earth element product stream varied from 80.2 wt% to 97.6 wt% based solely on solvent extraction. In comparison, uranium recovery into the same product steam fluctuated between 3.4 wt % and 62.5 wt% under all tested conditions.
(4) A statistically significant model was developed for uranium recovery prediction in solvent extraction, indicating that the extractant concentration, solution pH, and O/A ratio all played a critical role. A simultaneous increase in the solution pH, organic to aqueous phase ratio, and extractant concentration generated the best separation performance between uranium and rare earths.
(5) The lowest overall uranium recovery of 1.8 wt% into the final product stream was achieved with 50 v% TBP, feed pH at 3.5, O/A ratio at 3, and 1 mol/L H_2SO_4 as the stripping agent, corresponding to an overall rare earth recovery of 73.4 wt%.
(6) On the contrary, the stripping agent (H_2SO_4) concentration was an insignificant parameter over the tested concentration range, which indicates that the TBP-U bonds were easy to break, transferring the uranium ions back into the aqueous phase. One mol/L H_2SO_4 was sufficient for the uranium stripping purpose.
(7) Following detailed parametric tests, performance validation tests were conducted on the rare earth oxalate sample produced from a pilot-scale processing facility. Test results validate the efficiency and reliability of the separation protocol developed. A five-stage conceptual flowsheet was thus proposed to shed light on technology development to eventually utilize coal and coal by-products to produce critical rare earths.

Highlights

- A conceptual process was developed to separate Th and U from REEs.
- A coal-based feedstock was utilized in this study.
- Precipitation and extraction mechanisms were assessed with respect to fundamental studies.
- 73.4 wt% REEs, 0% Th and 1.8 wt% U were obtained in the final product stream.
- Statistical analyses were performed to investigate the separation performance.

Acknowledgments

The findings presented in this manuscript were based on a study that was supported by the Department of Energy under Award Number DE-FE0027035. Disclaimer: This report was prepared as an account of work sponsored by an agency of the United States Government. Neither the United States Government nor any agency thereof, nor any of their employees, makes any warranty, express or implied, or assumes any legal liability or responsibility for the accuracy, completeness, or usefulness of any information, apparatus, product, or process disclosed, or represents that its use would not infringe privately owned rights. Reference herein to any specific commercial product, process, or service by trade name, trademark, manufacturer, or otherwise does not necessarily constitute or imply its endorsement, recommendation, or favoring by the United States Government or any agency thereof. The view and opinions of authors expressed herein do not necessarily state or reflect those of the United States Government or any agency thereof.

The authors would like to express their gratitude towards the Department of Mining Engineering at the University of Kentucky and the National Research Center for Coal and Energy (NRCCE) at West Virginia University for the elemental analysis reported in this study.

Disclosure statement

No potential conflict of interest was reported by the author(s)

Funding

This work was supported by the Department of Energy National Energy Technology Laboratory [DE-FE0027035].

ORCID

Deniz Talan http://orcid.org/0000-0003-0640-1414

Preferred reviewers

(1) Dr. Rick Honaker, University of Kentucky, rick.honaker@uky.edu
(2) Dr. Aaron Noble, Virginia Polytechnic Institute and State University, aaron.noble@vt.edu
(3) Dr. Wencai Zhang, Virginia Polytechnic Institute and State University, wencaizhang@vt.edu
(4) Dr. Xinbo Yang, University of Kentucky, Xinbo.yang@uky.edu

References

Abaka-Wood, G., J. Adaai-Mensah, and W. Skinner. 2021. "The Use of Mining Tailings as Analog of Rare Earth Elements Resources: Part 1-Characterization and Preliminary Separation." *Mineral Processing and Extractive Metallurgy Review* 1547–7401.

Abdel-Sabour, M. 2014. "Uranium Fixation and Removal from Different Soil Types: Review." *Journal of Nuclear Energy Science and Power Generation Technology* 3:3.

Agarwal, V., M. Safarzade, and J. Galvin. 2018. "Solvent Extraction and Separation of Y(III) from Sulfate, Nitrate, and Chloride Solutions Using PC88A Diluted in Kerosene." *Mineral Processing and Extractive Metallurgy Review* 39 (4):258–65. doi:10.1080/08827508.2017.1415210.

Akcil, A., N. Akhmediyeva, R. Abdulvaliyev, Abhilash, and P. Meshram. 2018. "Overview on Extraction and Separation of Rare Earth Elements from Red Mud." *Focus on Scandium. Mineral Processing and Extractive Metallurgy Review* 39 (3):145–51. doi:10.1080/08827508.2017.1288116.

Al-Areqi, W., A. Majid, and S. Sarmani (2014). "Thorium, Uranium, and Rare Earth Elements Content in Lanthanide Concentrate (LC) and Water Leach Purification (WLP) Residue of Lynas Advanced Materials Plant (LAMP)." *American Institute of Physics Conference Proceedings*, Malaysia, 93–96. doi:10.1063/1.4866110.

Al-Thyabat, S., and P. Zhang. 2015. "REE Extraction from Phosphoric Acid, Phosphoric Acid Sludge, and Phosphogypsum." *Mineral Processing and Extractive Metallurgy, Transactions of the Institutions of Mining and Metallurgy: Section C* 124 (3):143–50. doi:10.1179/1743285515Y.0000000002.

Amaral, J., and C. Morais. 2010. "Thorium and Uranium Extraction from Rare Earth Elements in Monazite Sulfuric Acid Liquor Through Solvent Extraction." *Minerals Engineering* 23 (6):498–503. doi:10.1016/j.mineng.2010.01.003.

Amer, T., W. Abdeall, G. Abdel Wahab, and E. El-Sheikh. 2013. "A Suggested Alternative Procedure for Processing of Monazite Mineral Concentrate." *International Journal of Mineral Processing* 125:106–11. doi:10.1016/j.minpro.2013.10.004.

Ault, T., S. Krahn, and A. Croff. 2015. "Radiological Impacts and Regulations of Rare Earth Elements in Non-Nuclear Energy Production." *Energies* 8 (3):2066–81. doi:10.3390/en8032066.

Baek, D., R. Fox, M. Case, L. Sinclair, A. Schmidt, P. McIlwain, and C. Wai. 2016. "Extraction of Rare Earth Oxides Using Supercritical Carbon Dioxide Modified with Tri- n -Butyl Phosphate–Nitric Acid Adducts." *Industrial and Engineering Chemistry Research* 55 (26):7154–63. doi:10.1021/acs.iecr.6b00554.

Balintova, M., and A. Petrilakova. 2011. "Study of pH Influence on Selective Precipitation of Heavy Metals from Acid Mine Drainage." *Chemical Engineering Transactions* 25:345–50.

Belova, V., N. Egorova, A. Voshkin, and A. Khol'kin. 2015. "Extraction of Rare Earth Metals, Uranium and Thorium from Nitrate Solutions by Binary Extractants." *Theoretical Foundations of Chemical Engineering* 49 (4):545–49. doi:10.1134/S0040579515040041.

Binnemans, K., P. Jones, B. Blanpain, T. Gerven, Y. Yang, A. Walton, and M. Buchert. 2013. "Recycling of Rare Earths: A Critical Review." *Journal of Cleaner Production* 51:1–22. doi:10.1016/j.jclepro.2012.12.037.

Biswas, S., P. Pathak, D. Singh, and S. Roy. 2013. "Comparative Evaluation of Tri- n -butyl Phosphate (TBP) and Tris(2-ethylhexyl) Phosphate (TEHP) for the Recovery of Uranium from Monazite Leach Solution". *Separation Science and Technology* 48 (13):2013–19. doi:10.1080/01496395.2013.790449.

Braatz, A., M. Antonio, and M. Nilsson. 2017. "Structural Study of Complexes Formed by Acidic and Neutral Organophosphorus Reagents." *Dalton Transactions* 46 (4):1194–206. doi:10.1039/C6DT04305D.

Brookins, D. 1988. *Eh-pH Diagrams for Geochemistry*. Albuquerque: Springer-Verlag.

Brown, C., and L. Sherrington. 1979. "Solvent Extraction used in Industrial Separation of Rare Earths." *Journal of Chemical Technology and Biotechnology* 29:193–209. doi:10.1002/jctb.503290402.

Choppin, G., and M. Khankhasayev. 1998. *Chemical Separation Technologies and Related Methods of Nuclear Waste Management: Applications, Problems and Research Needs*. The Netherlands: Kluwer Academic Publishers.

Cooper, M. 2005. *Naturally Occurring Radioactive Materials (NORM) in Australian Industries - Review of Current Inventories and Future Generation*. Australia: Radiation Health and Safety Advisor Council.

Dai, S., and R. Finkelman. 2018. "Coal As A Promising Source of Critical Elements: Progress and Future Prospects." *International Journal of Coal Geology* 186:155–64. doi:10.1016/j.coal.2017.06.005.

Dutta, T., K. Kim, M. Uchimiya, E. Kwon, B. Jeon, A. Deep, and S. Yun. 2016. "Global Demand for Rare Earth Resources and Strategies for Green Mining." *Environmental Research* 150:182–90. doi:10.1016/j.envres.2016.05.052.

Erust, C., A. Akcil, A. Tuncuk, H. Deveci, and E. Yazici. 2021. "A Multi-Stage Process for Recovery of Neodymium (Nd) and Dysprosium (Dy) from Hard Disc Drives (HDDs)." *Mineral Processing and Extractive Metallurgy Review* 42 (2):90–101. doi:10.1080/08827508.2019.1692010.

Eskanazy, G. 1987. "Rare Earth Elements and Yttrium in Lithotypes of Bulgarian Coals." *Org Geochem* 11(2): 83–89.

Eskanlou, A., and Q. Huang. 2021. "Phosphatic waste clay: Origin, composition, physicochemical properties, challenges, values and possible remedies–A review." *Minerals Engineering* 162:106745.

Felmy, A., D. Rai, and M. Mason. 1991. "The Solubility of Hydrous Thorium(IV) Oxide in Chloride Media: Development of An Aqueous Ion-InteRadiochimica Actaion Model." *Radiochimica Acta* 55 (4):177–85.

Ferron, C., and P. Henry. 2015. "A Review of the Recycling of Rare Earth Metals." *Canadian Metallurgical Quarterly* 54 (4):388–94. doi:10.1179/1879139515Y.0000000023.

Findeib, M., and A. Schaffer. 2017. "Fate and Environmental Impact of Thorium Residues During Rare Earth Processing." *Journal of Sustainable Metallurgy* 3 (1):179–89. doi:10.1007/s40831-016-0083-3.

Finkelman, R. 1999. "Trace Elements in Coal Environmental and Health Significance." *Biological Trace Element Research* 67 (3):197–204. *Biological Trace Element Research*. doi:10.1007/BF02784420.

Garcia, A., M. Latifi, A. Amini, and J. Chaouki. 2020. "Separation of Radioactive Elements from Rare Earth Element-Bearing Minerals." *Metals* 10 (11):1524. doi:10.3390/met10111524.

Giri, R., and G. Nath. 2016. "Physicochemical Study of Extractants for Extraction of Rare Earth Element." *Journal of Analytical Science and Technology* 7 (1). doi:10.1186/s40543-016-0101-x.

Gupta, B., P. Malik, and A. Deep. 2002. "Extraction of Uranium, Thorium and Lanthanides using Cyanex-923 Their Separations and Recovery from Monazite." *Journal of Radioanalytical and Nuclear Chemistry* 251 (3):451–56. doi:10.1023/A:1014890427073.

Habashi, F. 1997. *Handbook of Extractive Metallurgy*. Quebec: Wiley-VHC.

Haque, N., A. Hughes, S. Lim, and C. Vernon. 2014. "Rare Earth Elements: Overview of Mining, Mineralogy, Uses." *Sustainability and Environmental Impact. Resources* 3 (4): 614–35.

Hidayah, N., and S. Abidin. 2017. "The Evolution of Mineral Processing in Extraction of Rare Earth Elements Using Solid-Liquid Extraction over Liquid-Liquid Extraction - A Review." *Minerals Engineering* 112:103–13. doi:10.1016/j.mineng.2017.07.014.

Honaker, R., J. Groppo, A. Bhagavatula, M. Razaee, and W. Zhang. 2016. Coa Prep 2016, April 25-27, 2016, Louisville, KY.

Honaker, R., J. Hower, C. Eble, J. Weisenfluh, J. Groppo, M. Rezaee, and A. Bhagavatula. 2014. "Laboratory and Bench-Scale Testing for Rare Earth Elements." .

Honaker, R., W. Zhang, X. Yang, and M. Rezaee. 2018. "Conception of An Integrated Flowsheet for Rare Earth Elements Recovery from Coal Coarse Refuse." *Minerals Engineering* 122:233–40. doi:10.1016/j.mineng.2018.04.005.

Hower, J., E. Granite, D. Mayfield, A. Lewis, and R. Finkelman. 2016. "Notes on Contributions to the Science of Rare Earth Element Enrichment in Coal and Coal Combustion Byproducts." *Minerals* 6 (2):1–9.

Hu, J., B. Zheng, R. Finkelman, B. Wang, M. Wang, S. Li, and D. Wu. 2006. "Concentration and Distribution of Sixty-One Elements in Coals from DPR Korea." *Fuel* 85 (5–6):679–88. doi:10.1016/j.fuel.2005.08.037.

Huang, Q., A. Noble, J. Herbst, and R. Honaker. 2018. "Liberation and Release of Rare Earth Minerals from Middle Kittanning." *Fire Clay, and West Kentucky No* 13:242–52. Coal Sources. *Powder Technology*

Huang, Q., D. Talan, J. Restrepo, O. Baena, V. Kecojevic, and A. Noble. 2019. "Characterization Study of Rare Earths, Yttrium and Scandium from Various Colombian Coal Samples and Non-Coal Lithologies." *International Journal of Coal Geology* 209:14–26. doi:10.1016/j.coal.2019.04.008.

Hughes, K., and R. Singh. 1980. "The Isolation of Thorium from Monazite by Solvent Extraction." *Hydrometallurgy* 6 (1–2):25–33. doi:10.1016/0304-386X(80)90005-5.

IAEA. 2000. *Recycle and Reuse of Materials and Components from Waste Streams of Nuclear Fuel Cycle Facilities*. Austria: IAEA.

Ismail, N., M. Aziz, M. Yunus, and A. Hisyam. 2019. "Selection of Extractant in Rare Earth Solvent Extraction System: A Review." *International Journal of Recent Technology and Engineering* 8 (1):728–43.

Jha, M., A. Kumari, R. Panda, J. Kumar, K. Yoo, and J. Lee. 2016. "Review on Hydrometallurgical Recovery of Rare Earth Metals." *Hydrometallurgy* 165:2–26. doi:10.1016/j.hydromet.2016.01.035.

Jorjani, E., and M. Shahbazi. 2012. "The Production of Rare Earth Elements Group via Tributyl Phosphate Extraction and Precipitation Stripping Using Oxalic Acid." *Arabian Journal of Chemistry* 9:1532–39. doi:10.1016/j.arabjc.2012.04.002.

Karayigit, A., R. Gayer, X. Querol, and T. Onacak. 2000. "Contents of Major and Trace Elements in Feed Coals from Turkish Coal-Fired Power Plants." *International Journal of Coal Geology* 44 (2):169–84. doi:10.1016/S0166-5162(00)00009-4.

Kawatra, S. 2020. *Advanced Coal Preparation and Beyond: CO2 Capture and Utilization*. Boca Raton: CRC Press.

Ketris, M., and Y. Yudovich. 2009. "Estimations of Clarkes for Carbonaceous Biolithes: World Averages for Trace Element Contents in Black Shales and Coals." *International Journal of Coal Geology* 78 (2):135–48. doi:10.1016/j.coal.2009.01.002.

Kim, E., and K. Osseo-Asare. 2012. "Aqueous Stability of Thorium and Rare Earth Metals in Monazite Hydrometallurgy: Eh-pH Diagrams for the Systems T-, Ce-, La-, Nd-, (PO4)-(SO4)-H2O at 25C." *Hydrometallurgy* 113-114:67–78. doi:10.1016/j.hydromet.2011.12.007.

Kuang, S., Z. Zhang, Y. Li, H. Wei, and W. Liao. 2017. "Synergistic Extraction and Separation of Rare Earths from Chloride Medium by the Mixture of HEHAPP and D2EHPA." *Hydrometallurgy* 174:78–83. doi:10.1016/j.hydromet.2017.09.011.

Lange, C., I. Camargo, A. Figueiredo, L. Castro, M. Vasconcellos, and R. Ticianelli. 2017. "A Brazilian Coal Fly Ash as a Potential Source of Rare Earth Elements." *Journal of Radioanalytical and Nuclear Chemistry* 311 (2):1235–41. doi:10.1007/s10967-016-5026-8.

Langmuir, D. 1978. "Uranium Solution-Mineral Equilibria at Low Temperatures with Applications to Sedimentary Ore Deposits." *Geochimica et Cosmochimica Acta* 42 (6):547–69. doi:10.1016/0016-7037(78)90001-7.

McLellan, B., G. Corder, A. Golev, and S. Ali. 2014. "Sustainability of the Rare Earths Industry." *Procedia Environmental Sciences* 20:280–87. doi:10.1016/j.proenv.2014.03.035.

Menzies, I., and F. Rigby. 1961. "Separation of Thorium from Uranium and Rare Earth Elements by Solvent Extraction with Tri-n-Butyl Phosphate-Xylene." *J. Appl. Chem* 11:104–13. doi:10.1002/jctb.5010110305.

Monji, A., V. Ghoulipour, and M. Mallah. 2016. "Selective Sorption of Uranium (IV) from Hydrochloric Acid Media by Agro-Industrial Byproducts." *Annals of Nuclear Energy* 97:115–21. doi:10.1016/j.anucene.2016.06.032.

Nasab, M., A. Sam, and S. Milani. 2011. "Determination of Optimum Process Conditions for the Separation of Thorium and Rare Earth Elements by Solvent Extraction." *Hydrometallurgy* 106 (3–4):141–47. doi:10.1016/j.hydromet.2010.12.014.

Neck, V., and J. Kim. 2001. "Solubility and Hydrolysis of Tetravalent Actinides." *Radiochimica Acta* 89 (1):1–16. doi:10.1524/ract.2001.89.1.001.

Orabi, A. 2013. "Determination of Uranium After Separation Using Solvent Extraction from Slightly Nitric Acid Solution and Spectrophotometric Detection." *Journal of Radiation Research and Applied Sciences* 6 (2):1–10. doi:10.1016/j.jrras.2013.09.001.

Palmieri, H., E. Knupp, L. Auler, L. Gomes, and C. Windmoller (2011). "Direct Quantification of Thorium." Uranium and Rare Earth Element Concentrations in Natural Waters by ICP-MS.*2011 International Nuclear Atlantic Conference*. Brazil.

Pan, J., C. Zhou, M. Tang, S. Cao, C. Liu, N. Zhang, . . . W. Ji. 2019. "Study on the Modes of Occurrence of Rare Earth Elements in Coal Fly Ash by Statistics and A Sequential Chemical Extraction Process." *Fuel* 555–65.

Papastefanou, C. 2007. "Radioactivity of Coals and Fly Ashes." *Journal of Radioanalytical and Nuclear Chemistry* 275:29–35.

Parzentny, H., and L. Rog. 2019. "The Role of Mineral Matter in Concentrating Uranium and Thorium in Coal and Combustion Residues from Power Plants in Poland." *Minerals* 9 (5):312. doi:10.3390/min9050312.

Paulick, H., and E. Machacek. 2017. "The Global Rare Earth Element Exploration Boom: An Analysis of Resources Outside of China and Discussion of Development Perspectives." *Resources Policy* 52:134–53. doi:10.1016/j.resourpol.2017.02.002.

Peiro, L., and G. Mendez. 2013. "Material and Energy Requirement for Rare Earth Production." *JOM* 65 (10):1327–40. doi:10.1007/s11837-013-0719-8.

Peramaki, S. (2012). *Method Development for Determination and Recovery of Rare Earth Elements from Industrial Fly Ash*. Thesis, University of Jyvaskyla.

Pillai, P. (2007). "Naturally Occurring Radioactive Materials (NORM) in the Extraction and Processing of Rare Earths." *Proceedings of An International Symposium* (pp. 197–221). Seville, Spain: International Atomic Energy Agency.

Ponou, J., G. Dodbiba, J. Anh, and T. Fujita. 2016. "Selective Recovery of Rare Earth Elements from Aqueous Solution Obtained from Coal Power Plant Ash." *Journal of Environmental Chemical Engineering* 4 (4):3761–66. doi:10.1016/j.jece.2016.08.019.

Preira, H., L. Frescura, B. Menezes, R. Duarte, M. Villetti, M. Hilgemann, and M. Rosa. 2019 AMultivariate Approach at the Thermodynamic Properties of Rare Earth Elements. *Thermochimica Acta* 678 (30):178315.

Qi, D. 2018. "Extractants Used in Solvent Extraction-Separation of Rare Earths: Extraction Mechanism, Properties, and Features." In *Hydrometallurgy of Rare Earths-Separation and Extraction*,187–389. 1st ed. Elsevier. https://doi.org/10.1016/B978-0-12-813920-2.00002-7

Reddy, M., T. Prasada Rao, and A. Damodaran. 1995. "Liquid-liquid Extraction Processes for the Separation and Purification of Rare Earths." *Mineral Processing and Extractive Metallurgy Review* 12 (2–4): 91–113.

Schreiber, A., J. Marx, P. Zapp, J. Hake, D. Vobenkaul, and B. Friedrich. 2016. "Environmental Impacts of Rare Earth Mining and Separation Based on Eudialyte: A New European Way." *Resources* 5 (4):32. doi:10.3390/resources5040032.

Stevenson, P., and W. Nervik. 1961. *The Radiochemistry of the Rare Earths, Scandium, Yttrium and Actinium*. Washington DC, the USA: National Academy of Sciences, National Research Council, Nuclear Science Series.

Suli, I., Ibrahim, W., Aziz, B., Deraman, M., Ismail, N.2017. A Review of Rare Earth Mineral Processing Technology *Chem. Eng. Res. Bullet*. 19:20–35.

Talan, D., and Q. Huang. 2020. "Separation of Thorium, Uranium and Rare Earths from A Strip Solution Generated from Coarse Coal Refuse." *Hydrometallurgy* 197:105446. https://doi.org/10.1016/j.hydromet.2020.105446

Thakur, N. 2000. "Separation of Rare Earths by Solvent Extraction." *Mineral Processing and Extractive Metallurgy Review* 21 (1–5):277–306. doi:10.1080/08827500008914171.

United States Geological Survey. (1997). "Retrieved from Radioactive Elements in Coal and Fly Ash: Abundance, Forms, and Environmental Significance." Fact Sheet FS 163–97.

Valkov, A., V. Sergievskiy, V. Sofronov, M. Kalaev, and Y. Ermakova. 2014. "Studies in the Field of Rare Earth Elements." *Procedia Chemistry* 11:171–75. doi:10.1016/j.proche.2014.11.030.

Van Gosen, B., P. Verplanck, R. Seal, K. Long, and J. Gambogi. 2017. "Rare-Earth Elements, Chapter O of." In *Critical Mineral Resources of the United States-Economic and Environmental Geology and Prospects for Future Supply: U.S. Geological Survey Professional Paper*, ed. K. J. Schulz, J. H. DeYoung, R. R. Seal, and D. C. Bradley. Virginia: U.S.G.S. O1–O31.

Wagner, N., and A. Matiane. 2018. "Rare Earth Elements in Select Main Karoo Basin (South Africa) Coal and Coal Ash Samples." *International Journal of Coal Geology* 196:82–92. doi:10.1016/j.coal.2018.06.020.

Wang, L., X. Huang, Y. Yu, L. Zhao, C. Wang, and Z. Feng. 2017. "Towards Cleaner Production of Rare Earth Elements from Bastnaesite in China." *Journal of Cleaner Production* 165:231–42. doi:10.1016/j.jclepro.2017.07.107.

Xie, F., T. Zhang, D. Dreisinger, and F. Doyle. 2014. "A Critical Review on Solvent Extraction of Rare Earths from Aqueous Solutions." *Minerals Engineering* 56:10–28. doi:10.1016/j.mineng.2013.10.021.

Yang, J., S. Montross, J. Britton, M. Stuckman, C. Lopano, and C. Verba. 2020. "Microanalytical Approached to Characterizing REE in Appalachian Basin Underclays." *Minerals* 10 (6):546. doi:10.3390/min10060546.

Yang, Y., X. Zhang, L. Li, T. Wei, and K. Li. 2019. "Metastable Dissolution Regularity of Nd 3+ in Na 2 CO 3 Solution and Mechanism in Na2CO3 Solution and Mechanism." *ACS Omega* 4 (5):9160–68. doi:10.1021/acsomega.9b00453.

Zhang, W., and R. Honaker. 2018. "Rare Earth Elements Recovery Using Stages Precipitation from A Leachate Generated from Coarse Coal Refuse." *International Journal of Coal Geology* 195:189–99. doi:10.1016/j.coal.2018.06.008.

Zhang, W., and R. Honaker (2019). USA Patent No. 2019/0136344.

Zhang, J., B. Zhao, and B. Schreiner. 2016. *Separation Hydrometallurgy of Rare Earth Elements*. Saskatoon: Springer.

Zhou, H., Y. Wang, X. Guo, Y. Dong, X. Su, and X. Sun. 2018. "The Recovery of Rare Earth by A Novel Extraction and Precipitation Strategy using Functional Ionic Liquids." *Journal of Molecular Liquids* 254:414–20. doi:10.1016/j.molliq.2018.01.078.

Zhu, Z., Y. Pranolo, and C. Cheng. 2015. "Separation of Uranium and Thorium from Rare Earths for Rare Earth Production - A Review." *Minerals Engineering* 77:185–96. doi:10.1016/j.mineng.2015.03.012.